Environmental Science & Technology

pubs.acs.org/est

Article

Contrasting Controls on the Diel Isotopic Variation of Hg^0 at Two High Elevation Sites in the Western United States

Aaron Y. Kurz,* Joel D. Blum, Lynne E. Gratz, and Daniel A. Jaffe

Cite This: *Environ. Sci. Technol.* 2020, 54, 10502−10513

Read Online

ACCESS | Metrics & More | Article Recommendations | Supporting Information

ABSTRACT: The atmosphere is a significant global reservoir for mercury (Hg) and its isotopic characterization is important to understand sources, distribution, and deposition of Hg to the Earth's surface. To better understand Hg isotope variability in the remote background atmosphere, we collected continuous 12-h Hg^0 samples for 1 week from two high elevation sites, Camp Davis, Wyoming (valley), and Mount Bachelor, Oregon (mountaintop). The samples collected at Camp Davis displayed strong diel variation in δ^{202}Hg values of Hg^0, but not in Δ^{199}Hg or Δ^{200}Hg values. We attribute this pattern to nightly atmospheric inversions trapping Hg in the valley and the subsequent nighttime uptake of Hg by vegetation, which depletes Hg from the atmosphere. At Mount Bachelor, the samples displayed diel variation in both δ^{202}Hg and Δ^{199}Hg, but not Δ^{200}Hg. We attribute this pattern to differences in the vertical distribution of Hg in the atmosphere as Mount Bachelor received free tropospheric air masses on certain nights during the sampling period. Near the end of the sampling period at Mount Bachelor, the observed diel pattern dissipated due to the influence of a nearby forest fire. The processes governing the Hg isotopic fractionation differ across sites depending on mixing, topography, and vegetation cover.

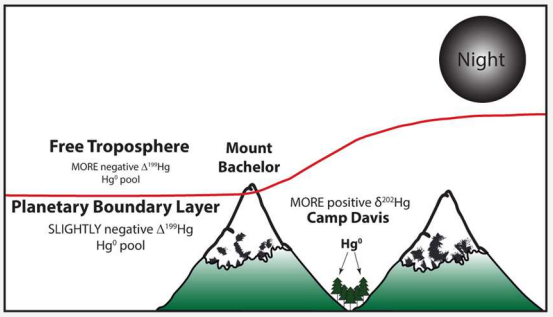

1. INTRODUCTION

Mercury (Hg) is a trace metal found ubiquitously at Earth's surface and in its atmosphere and is of concern to human health. Human activities such as combustion of fossil fuels and mining of mercury and gold have increased atmospheric Hg concentrations globally and altered the natural chemistry and cycling of Hg in the environment.[1−3] Active redox chemistry controls transitions between the different chemical species of Hg, which determines the cycling behavior and fate of Hg in the atmosphere.

Atmospheric Hg has three operationally defined species: gaseous elemental mercury (GEM; Hg^0), gaseous oxidized mercury (GOM; $Hg_{(g)}^{II}$), and particulate bound mercury (PBM; $Hg_{(p)}^{II}$). Together, GEM and GOM are defined as total gaseous mercury (TGM). Hg^0 is thought to be the dominant form of Hg in the atmosphere comprising >95% of the global pool.[4] Hg^0 is relatively nonreactive and has an atmospheric residence time of ∼1 year.[5,6] Hg^0 can undergo oxidation reactions and become $Hg_{(g)}^{II}$, which is thought to have an atmospheric residence time on the order of days to weeks.[7,8] $Hg_{(g)}^{II}$ can also adsorb to particles and is then defined as $Hg_{(p)}^{II}$, which also has an atmospheric residence time of days to weeks.[8]

The isotopic composition of atmospheric Hg pools has not been well studied due to the low concentrations of Hg species and the difficulties of sample collection. The large volumes of air needed to obtain enough Hg for isotopic analysis lead to most individual samples being integrated over time periods of 24-h to 2 weeks of continuous collection.[9,10] The lack of sampling and isotopic analysis of atmospheric Hg leaves a large knowledge gap in the specific reactions that govern Hg cycling in the atmosphere.[11] Recent advancements in multiple collector inductively coupled plasma mass spectrometry (MC-ICP-MS) allow for high precision measurements of mercury's seven stable isotopes.[12] Both experimental studies and environmental measurements have shed light on mercury cycling and the reactions and pathways that control Hg isotopic fractionation.[2]

The measurement of Hg stable isotope ratios is a powerful tool due to the fact that mercury displays both mass dependent fractionation (MDF) as well as mass independent fractionation (MIF).[13] MDF is controlled by both biotic and abiotic reactions including methylation, demethylation, photoreduction, and equilibrium reactions.[14−16] MIF is mainly controlled by reactions involving photochemistry.[17,18] The identification of these two types of fractionation aids in tracing Hg through the environment and enhancing understanding of changes in Hg speciation.[9,19−21]

Received: March 27, 2020
Revised: July 21, 2020
Accepted: July 31, 2020
Published: July 31, 2020

https://dx.doi.org/10.1021/acs.est.0c01918
Environ. Sci. Technol. 2020, 54, 10502−10513

Most atmospheric Hg isotopic measurements have been made at ground level and at low elevation but those studies made aloft have revealed that there is an altitudinal gradient of mercury concentration in the atmosphere and that there is also a shift from Hg^0 to $Hg_{(g)}^{II}$ dominance with increasing altitude.[22,23] This has led to speculation that the Hg species composition of the stratosphere could be different than that of the troposphere and that there may be a difference between the planetary boundary layer (PBL) and the free troposphere (FT). Along with a difference in Hg species throughout the atmospheric vertical column, there is also thought to be a difference in the isotopic composition of Hg.[24] The Hg isotopic composition measured in air masses is affected by the origin and trajectory. Measurements of Hg stable isotopes in atmospheric species allow for differentiation between point source, regional or background sources of Hg.[9,10,19] Additionally, recent studies have used the fractionation imparted on air masses by the uptake of Hg from the atmosphere by vegetation to understand the Hg isotopic composition of sampled TGM.[9,20,25] Most recently, Huang et al. collected 12-hr PBM samples in Beijing, China. These authors found that the daytime samples with increased exposure to sunlight had higher odd-MIF, which they attributed to in situ photoreduction.[26] Huang et al. represent the first measurements of day vs night samples for Hg isotopes in atmospheric samples. Jiskra et al. used integrated 12-hour samples of TGM at Toolik Lake Field Station in Alaska to assess differences between day and night samples. These authors found a difference in MDF between day and night samples and attributed this difference to the uptake and re-emission of Hg from vegetation.[27] This body of work provides an important start to understanding the different local and regional processes, reactions, and conditions that influence the isotopic composition of atmospheric Hg species.

To assess diel variations in Hg^0 isotopic composition and further characterize the global atmospheric Hg pool, we collected continuous 12-h Hg^0 samples over a 7-day period in the summer of 2019 at the University of Michigan Camp Davis Geological Field Station (Camp Davis), a forested high elevation site in the Hoback Mountains in Western Wyoming (Figure S1). Here, we expected the uptake of Hg by vegetation to dominate the diel variation in Hg^0. We additionally conducted a similar sampling campaign at the Mount Bachelor Observatory (MBO) near Bend, Oregon during the summer of 2017 (Figure S1). This high elevation site is far from any point source of Hg and often receives free tropospheric air masses on a nightly basis.[28] We hypothesized that there would be isotopic variation in both MDF and MIF between the day and night samples due to differences in the vertical distribution of Hg in the atmosphere. We expected differences in vegetation cover, meteorology, mixing, and redox chemistry to drive different diel patterns between the two high elevation study sites. This provides an opportunity to better understand the processes controlling the Hg isotopic composition at high elevation sites and further characterize the isotopic composition of mercury's vertical distribution in the atmosphere.

2. METHODS

2.1. Study Sites. Camp Davis (CD), is located in a valley in the Hoback Mountain Range in Western Wyoming at an elevation of 1872 m above sea level (43°16′55.11″N, 110°39′26.68″W). CD is situated at the base of Mt. Ann, whose peak is ∼2270m above sea level, on Quaternary aged alluvium. The Hoback River flows through the valley ∼1 km north of the sampling site. The sampling location is at the edge of a forest with lodgepole pine (*Pinus contorta*) and Douglas fir (*Pseudotsuga menziesii*; the dominant species). During the sampling period, temperatures ranged from 3 to 28 °C and sky conditions remained mostly clear with some intermittent clouds. Here, we collected 12-h Hg^0 samples continuously for 1 week (total of 13 samples) from June 26 to July 3, 2019.

The second high elevation sample site, the Mount Bachelor Observatory (MBO), is located on the leeward side of a dormant volcano (2734 m above the sea level) located in the Cascade Range approximately 30 km southwest of Bend, Oregon (43°58′39.19″ N, 121°41′9.66″ W). The site location is approximately 500 m above the tree line and 200 km east of the Pacific Ocean coastline and frequently receives FT air masses during the night.[28,29] During the sampling period, temperatures ranged from approximately 8 to 14 °C. Sky conditions remained clear throughout the sampling period. The surrounding valleys began to fill with smoke from the nearby Milli forest fire beginning on Aug 19 through the end of the sampling period. Here, we collected 12-hr Hg^0 samples continuously for 1 week (total of 13 samples) from Aug 15−22, 2017. MBO has been in operation since 2004, measuring atmospheric constituents such as CO, aerosol scattering, and Hg species as well as other basic meteorological parameters.[29,30] Through these measurements, MBO has been well characterized meteorologically and characteristic concentrations of atmospheric constituents have been measured during events such as forest fires, air masses dominated by long-range pollution transport from Asia, and free tropospheric air masses.[28,30−32] We can compare this long-term characterization with measurements taken during our sampling campaign to assess the impacts of the nearby forest fires and to estimate when FT air masses may have dominated our samples.

2.2. Hg^0 Sample Collection and Preparation. Our method of Hg^0 sample collection has been previously described in Demers et al. and Kurz et al. Briefly, atmospheric air was drawn through a manifold with 8 gold bead traps in parallel at a rate of 1.8 L/min per gold trap (14.4 L/min total). Upstream of each gold trap, a filter housing was outfitted with a prefired quartz filter to prevent particulates from accumulating on the gold bead traps. The gold bead traps were wrapped with heat tape and kept at a constant temperature of 50 °C to prevent water condensation during sample collection. A dry test meter (Schlumberger, Gallus 2000) connected in the sampling train was used to measure the volume of air drawn through the manifold. Air volumes were corrected to standard temperature and pressure using the method outlined by the Environmental Protection Agency Compendium Method IO-2.4.

We acknowledge that there may be some influence of $Hg_{(g)}^{II}$ in the samples collected in this study; however, the difference in the isotopic composition between Hg^0 and Hg^{II} (GOM + PBM) has been shown to be significant in previous studies.[10,26,33] The upstream quartz filter in our sampling stream prevents $Hg_{(p)}^{II}$ from accumulating on the gold bead traps, though the extent to which $Hg_{(g)}^{II}$ is excluded from our samples is unclear. Thus, based on the Hg isotopic composition of the measured samples in this study as compared to previously collected samples that have been demonstrated to be dominantly Hg^0,[10,33] we believe that our samples are dominated by Hg^0.

https://dx.doi.org/10.1021/acs.est.0c01918
Environ. Sci. Technol. 2020, 54, 10502−10513

After sample collection and in the laboratory at the University of Michigan, each of the 8 gold bead traps in a sample was individually heated to 500 °C over a 4-min period to desorb the Hg and retrap it on a single analytical gold trap (diatomaceous earth coated with gold). The analytical gold trap was then heated in a step-wise manner from 25 to 550 °C over a 3.5-h period. The released Hg was carried in a stream of argon and bubbled through a 24 g liquid trap containing a solution of 1% $KMnO_4$ dissolved in 10% H_2SO_4 (hereafter referred to as 1% $KMnO_4$). The samples were then partially reduced with 2% (w/w) of a 30% $NH_2OH{\cdot}HCl$ solution and an aliquot was measured for total mercury (THg) via cold vapor atomic fluorescence spectroscopy (CV-AFS).

A second sample purification step was performed with all samples, which included sample reduction with 20% (w/w) $SnCl_2$ and subsequent purge and trap into a fresh 5.5 g liquid trap of 1% $KMnO_4$. This step was performed to remove residual contaminants that may have been transferred from the heated gold bead traps and that might potentially produce matrix effects during analysis. For determination of final sample THg, the samples were partially reduced with 2% (w/w) of a 30% $NH_2OH{\cdot}HCl$ solution and an aliquot was measured for THg via CV-AFS. Overall sample recoveries during processing ranged from 91.0 to 103.0% with an average recovery of 96.1 ± 4.1% (1 SD, n = 26). Process standards consisting of UM-Almadèn were loaded onto gold bead traps by reducing prepared standards with 20% $SnCl_2$, which was subsequently pumped through one gold bead trap at a time at a flow rate of 0.5 L/min, while simultaneously monitoring breakthrough via atomic absorption spectroscopy. These process standards, consisting of 8 gold bead traps loaded with UM-Almadèn in the manner described above, were used to evaluate gold bead trapping efficiency and to monitor the quantitative recovery of Hg during processing. UM-Almadèn process standards were processed in tandem with the samples and had recoveries ranging from 92.9 to 98.9% with an average of 96.3 ± 2.3% (1 SD, n = 6).

2.3. Mercury Isotope Analyses. Hg isotope analyses were conducted at the University of Michigan using a cold vapor multiple collector inductively coupled plasma mass spectrometer (CV-MC-ICP-MS) (Nu Plasma). Prior to analyses, the samples were partially reduced with 2% (w/w) of a 30% $NH_2OH{\cdot}HCl$ solution. The samples were prepared to match the concentration of the NIST 3133 standard (within 5% relative concentration) for standard sample bracketing. The samples were introduced into the instrument using continuous flow cold vapor generation and the Hg in solution was reduced to Hg^0 with the introduction of a 2% $SnCl_2$ solution. The Hg^0 was introduced into the CV-MC-ICP-MS in a stream of Ar along with a dry aerosol Tl standard (NIST 987) produced by a desolvating nebulizer and used for mass bias correction.

We report Hg isotopic compositions using delta notation, in units of permil (‰), as follows

$$\delta^{xxx}\mathrm{Hg}(‰) = \{[(\Delta^{xxx}\mathrm{Hg}/^{198}\mathrm{Hg})_{\mathrm{unknown}} / (\Delta^{xxx}\mathrm{Hg}/^{198}\mathrm{Hg})_{\mathrm{NIST\ 3133}}] - 1\} \times 1000$$

where xxx represents the Hg isotope of 199, 200, 201, or 204 amu.[12]

MIF is the deviation from the calculated MDF based on the kinetic isotope effect and is reported using capital delta notation. Blum and Bergquist calculated β constants that can be used to calculate MIF of less than ±10‰

$$\Delta^{xxx}\mathrm{Hg} = \delta^{xxx}\mathrm{Hg} - (\delta^{202}\mathrm{Hg} \times \beta)$$

xxx represents the Hg isotope mass (199, 200, 201, 204) and β represents the calculated constant (0.252, 0.502. 0.752, 1.492, respectively).[12]

UM-Almadèn was run as a secondary standard with each set of samples to assess analytical uncertainty. The results for UM-Almadèn measurements are presented in Table S1 and are similar to long-term measurements in both the University of Michigan lab and others.[34] The Hg^0 samples were run at concentrations between 1.56 and 4.28 ng/g. Secondary reference materials were prepared in the same manner as the samples and run at the same concentration as unknown samples. Process Hg^0 blanks yielded between 62.2 and 198 pg of Hg with an average of 113.9 ± 46.3 pg (1 SD, n = 6), while field Hg^0 blanks yielded between 115.5 and 453.5 pg of Hg with an average of 217.3 ± 135.9 pg (1 SD, n = 5). Field blanks are more representative of the blank associated with collecting Hg^0 samples and represent <5% of Hg in the lowest concentration sample collected.

Analytical errors associated with the sample analyses for the isotopes are calculated as 2 standard deviations (SD) of the secondary UM-Almadèn standard measurements or 2 standard errors (SE) of process standard measurements depending on whichever is larger. The MBO sample set was analyzed in Aug of 2018 and the CD sample set was analyzed in Oct of 2019. In Oct of 2018, we experienced a two-fold increase in sensitivity in our CV-MC-ICP-MS due to the introduction of a modified phase separator design. We therefore calculate our analytical errors separately for each sample set (Table S1). For Hg^0 samples collected at MBO, we use the 2SE associated with our process UM-Almadèn measurements from 2018 to assign analytical uncertainty to these samples for all isotope ratios except for Δ^{199}Hg as follows: ±0.10‰ for δ^{202}Hg, ±0.10‰ for Δ^{204}Hg, ±0.05‰ for Δ^{201}Hg, and ±0.05‰ for Δ^{200}Hg. For Δ^{199}Hg, we use the 2SD associated with UM-Almadèn measurements from 2018, which is ±0.05‰. For Hg^0 samples collected at CD, we use the 2SD associated with our UM-Almadèn measurements from 2019 to assign analytical uncertainty to these samples for all isotope ratios except for Δ^{200}Hg as follows: ±0.06‰ for δ^{202}Hg, ±0.03‰ for Δ^{204}Hg, ±0.03‰ for Δ^{201}Hg, and ±0.08‰ for Δ^{199}Hg. For Δ^{200}Hg, we use the 2SE associated with the process UM-Almadèn measurements from 2019, which is ±0.06‰.

2.4. Ancillary Atmospheric Chemistry Measurements at MBO. During the sampling period at MBO, CO and CO_2 were measured using a Picarro G2502 Cavity Ring-Down Spectrometer. Relative humidity (RH) was measured with a Campbell Scientific HMP 45C RH probe. Aerosol scattering (σ_{sp}) was measured at 3 different wavelengths (450, 550, and 700 nm) with an integrating nephelometer (TSI, Inc. Model 3563). Finally, particle mass was measured using a Grimm Technologies Model EDM 180 Optical Particle Counter (OPC). These measurements are described in previous publications.[31,35−37]

2.5. Atmospheric Transport. Hybrid Single-Particle Lagrangian Integrated Trajectory (HYSPLIT) models were run to assess air mass origin for the samples collected at both CD and MBO. The National Oceanic and Atmospheric Administration (NOAA) HYSPLIT model was run using the archived High-Resolution Rapid Refresh (HRRR) data with a grid resolution of 3 km × 3 km. Back trajectories with 24-hr durations were calculated every 12-h at the mid-time of each

https://dx.doi.org/10.1021/acs.est.0c01918
Environ. Sci. Technol. 2020, 54, 10502−10513

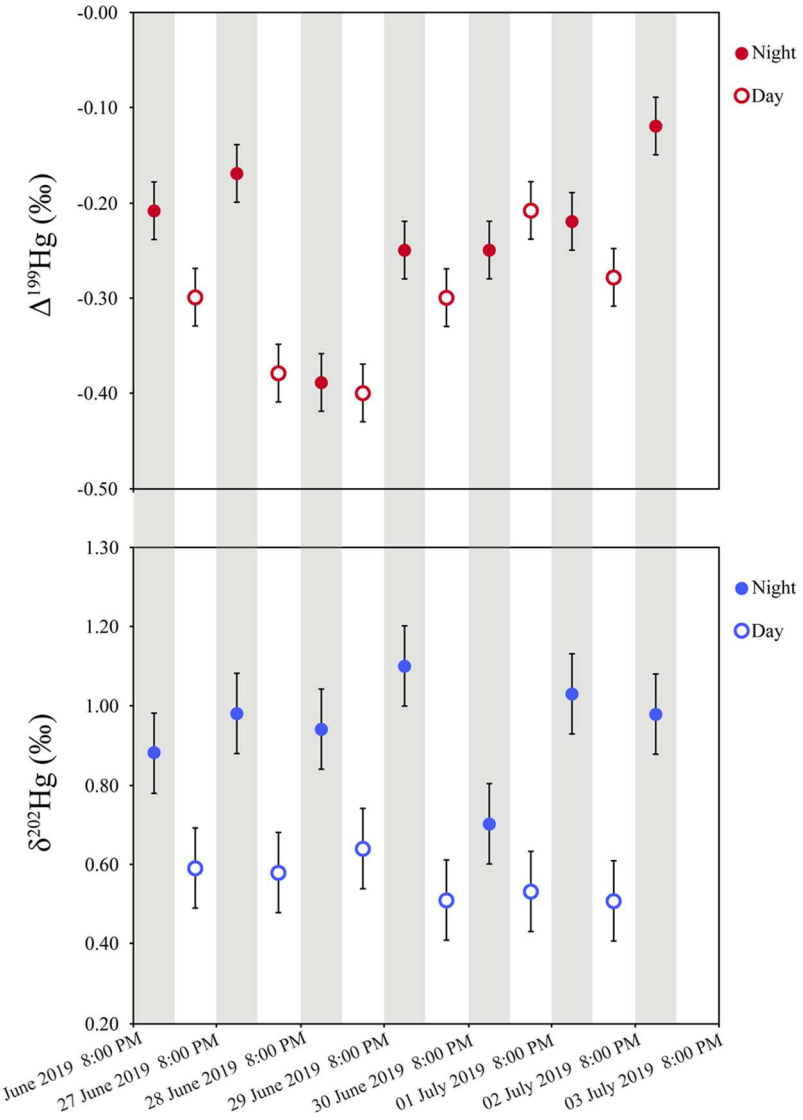

Figure 1. Camp Davis Hg isotope data plotted with δ^{202}Hg and Δ^{199}Hg on separate y-axes while sharing time on the *x*-axis. Vertical gray shading represents nighttime periods and white represents daytime. The black bars represent the analytical error (2SD).

sample with starting heights of 500, 1000, and 1500 m above ground level. The 24-h duration of back trajectories was chosen to provide a representative regional transport of Hg prior to each sample. Additionally, stability plots using the HRRR data set were generated to assess atmospheric stability and boundary layer heights during the sampling periods.[38,39]

2.6. Statistical Tests. All statistical tests employed in this study are independent two sample *t*-tests with equal variance at the 95% confidence interval and were calculated using RStudio (Version 1.2.5001, 2009-2019 RStudio, Inc.). All *t*-test results are presented in Table S2. All regressions were done using the York regression (York, 1968) and were also calculated using RStudio.

3. RESULTS AND DISCUSSION

3.1. Camp Davis THg Concentrations and Isotopic Compositions of Hg^0. CD Hg^0 sample THg concentrations range from 0.81 to 1.22 ng/m^3 over the entire sampling period. The samples collected during the day were characterized by higher average THg (1.06 ± 0.14 ng/m^3, 1 SD, n = 6) compared to those collected at night (0.94 ± 0.11 ng/m^3, 1 SD, n = 7) (Figure S2A), though these averages are not statistically different. The maximum THg concentration was recorded on July 1 (1.22 ng/m^3) and the lowest THg concentration was recorded on the night of June 29 (0.81 ng/m^3). The relative difference between the maximum and minimum measured THg concentrations was 34%. Modeled air mass back trajectories for the day and night samples indicated a regionally consistent origin before reaching CD (Figure S3). This suggests a constant, dominant source of Hg^0 to the sampling site that is representative of the regional Hg sources.

While the reported THg of Hg^0 samples is lower than Northern Hemisphere background Hg^0,[40−42] they are similar to THg concentrations measured in forested areas where similar diel patterns in Hg^0 concentrations have been observed.[43−45] These diel patterns have been attributed to differences in source, meteorology, uptake by vegetation, photoreduction/oxidation rate, and dry deposition.[43−45] The discussion below provides information concerning the use of Hg stable isotopes in elucidating the dominant processes causing diel variations in Hg^0.

https://dx.doi.org/10.1021/acs.est.0c01918
Environ. Sci. Technol. 2020, 54, 10502−10513

In the CD sample set, we recorded higher values of δ^{202}Hg during the night (average δ^{202}Hg = 0.94 ± 0.13‰, 1 SD, n = 7) with a maximum value of 1.10 ± 0.06‰ and lower values during the day (average δ^{202}Hg = 0.56 ± 0.05‰, 1 SD, n = 6) with a minimum value of 0.51 ± 0.06‰ (Figure 1). The day and night samples at CD are statistically different (Table S2).

Measurement of odd-MIF has proven to be a powerful tool in elucidating chemical transformations of Hg in the environment. Due to the fact that MIF of the odd mass Hg isotopes is mainly caused by photochemical reactions, measurements of Δ^{199}Hg and Δ^{201}Hg can help identify fractionation processes and trace Hg sources. Daytime Hg^0 measurements of Δ^{199}Hg and Δ^{201}Hg yielded average values of −0.31 ± 0.07 and −0.27 ± 0.07‰, respectively (1 SD, n = 6) (Figure 1). Nighttime samples yielded average values of −0.23 ± 0.08 and −0.26 ± 0.11‰, respectively (1 SD, n = 7). The averages between day and night samples are not statistically different for Δ^{199}Hg or Δ^{201}Hg (Table S2). While there is no consistent pattern in MIF values between day and night samples, there is a range of 0.28‰ between the highest and lowest recorded Δ^{199}Hg values during the sampling period. Additionally, there are days where daytime Δ^{199}Hg values are significantly lower than those of the previous or following night (June 27 and 28, and July 2) (Figure 1). The absence of a strong diel pattern in the odd-MIF of Hg^0 suggests that while there may be some influence from photochemical processes, other processes may also influence Hg concentration and isotopic variation.

3.2. Processes Driving Diel Variation in Hg^0 Isotopic Composition at Camp Davis. We identify four possible processes that control the diel variation of the Hg isotopic composition of Hg^0 measured at CD: (1) uptake of Hg^0 by vegetation, (2) deposition of Hg^0 to soil, (3) photoreduction of Hg^{II} and subsequent re-emission of Hg^0 from vegetation and/or soil, and (4) downward mixing of overlying air.[27,44−46]

3.2.1. Uptake of Hg^0 by Vegetation. Using a mixing model (described in the SI), we calculate the δ^{202}Hg value of the Hg that is lost from the atmosphere at night to be approximately −2.51‰ (eq S1). This value is similar to the δ^{202}Hg measurements of vegetation previously made in the region (−2.89‰).[3] Multiple environmental studies have documented a shift in atmospheric δ^{202}Hg values associated with vegetation uptake of Hg^0, where the MDF between Hg^0 and vegetation ranges from approximately −2.89 to −2.40‰.[20,25,47] This fractionation process has been shown to have both regional and global implications for the isotopic composition of Hg^0 in the atmosphere.[20,46,48]

CD is located in a valley in the Hoback Range and exhibits local scale meteorology characteristic of mountain valleys. Stability plots generated using NOAA's HRRR model indicate that during each night of the sampling campaign, atmospheric inversions occurred, creating a moderately stable to extremely stable (Pasquill atmospheric stability class) boundary layer in the valley with a depth of approximately 50−100 m (Figure S4A). These conditions are consistent with the documented trapping of chemical constituents, such as ozone and carbonyl sulfide, within the boundary layer and their depletion by chemical reactions or by vegetation uptake.[49,50] Hg^0 is an additional atmospheric constituent that is similarly trapped within the boundary layer resulting in diel variations in the THg and Hg isotopic composition.[27,43−45,47] During the day, solar radiation warms the ground, creating slightly to moderately unstable atmospheric conditions with a boundary layer depth of approximately 3000 m (Figure S4B). This allows overlying air to mix downward and to resupply Hg^0 to the valley. As a result of this behavior, the daytime samples display lower δ^{202}Hg and higher THg than those measured at night.

Hg^0 atmospheric THg concentrations in forests have been shown to be anticorrelated with light intensity, displaying minimum THg concentrations just before sunrise and maximum THg concentrations in the afternoon.[27,43−46,51] This is proposed to be a balance between vegetation uptake and re-emission and is documented by Hg flux measurements in forested areas.[43−45] We suggest that the lower Hg^0 THg concentrations and more positive δ^{202}Hg observed in the nighttime samples are characteristic of vegetation uptake of Hg^0, where the light isotopes are preferentially taken up by vegetation, leaving the residual Hg^0 in the atmosphere with heavier δ^{202}Hg values.[27]

3.2.2. Deposition of Hg^0 to Soil. Demers et al. found that as atmospheric air flowed through or interacted with surface soils, light isotopes were preferentially adsorbed or oxidized and removed from the atmosphere, leaving the residual Hg^0 pool with lower THg and higher δ^{202}Hg values. This process is thought to be similar to that of uptake of Hg^0 by vegetation and drives the MDF of Hg^0 in the atmosphere in the same direction. This process could contribute to the diel variation in THg and δ^{202}Hg, enhancing the effects of vegetation uptake on the residual atmospheric Hg^0 pool.

3.2.3. Photochemical Reduction of Hg^{II}. Experimental work on Hg isotopes has revealed diagnostic odd-MIF ratios that can be useful in identifying dominant redox reactions. Bergquist and Blum found that when Hg^{II} is photoreduced in the presence of DOM in an aqueous solution, the reactant is imparted with a Δ^{199}Hg/Δ^{201}Hg ratio of 1.00 ± 0.02.[52] Similarly, Sun et al. performed gas-phase experiments where they oxidized gaseous Hg with Cl and Br radicals. These reactions produced Δ^{199}Hg/Δ^{201}Hg ratios of 1.64 ± 0.30 and 1.89 ± 0.18 with the two different oxidants, respectively.[53] When either all of the CD data or only the nighttime samples are regressed using a York regression,[54] we calculate slopes of 0.31 ± 0.23 and 0.19 ± 0.28, which are both significantly lower than either oxidation or reduction experiments and do not indicate statistical significance (r^2 = 0.34, p > 0.3 and r^2 = 0.22, p > 0.2, respectively). However, when only the daytime data are regressed, we obtain a Δ^{199}Hg/Δ^{201}Hg slope of 0.82 ± 0.34 (r^2 = 0.90, p < 0.1), which overlaps with the experimental slope for Hg^{II} photoreduction. The difference in the slope between the regressions of all CD samples, only nighttime samples, and only daytime samples indicates a relative increase in the influence of photochemical reduction on the odd-MIF signatures during the day (Figure S5). This suggests that during the day, photoreduction of Hg^{II} plays a more important role in controlling Hg speciation than at night and could account for the differences in Δ^{199}Hg between the day and night samples of June 27 and 28 and July 2. The variation in the difference in Δ^{199}Hg values may be due to the magnitude of photoreduction and subsequent re-emission of Hg^0, though cannot be fully explained through variations in photoreduction.

3.2.4. Three-Endmember Mixing Model. Previous studies have utilized three-endmember mixing models to identify Hg source contributions in measured samples.[55,56] Here, we present a three-endmember mixing model that can account for the isotopic variation in the samples collected at CD. In Figure S6, we present a plot of δ^{202}Hg vs Δ^{199}Hg on the panel

https://dx.doi.org/10.1021/acs.est.0c01918
Environ. Sci. Technol. 2020, 54, 10502−10513

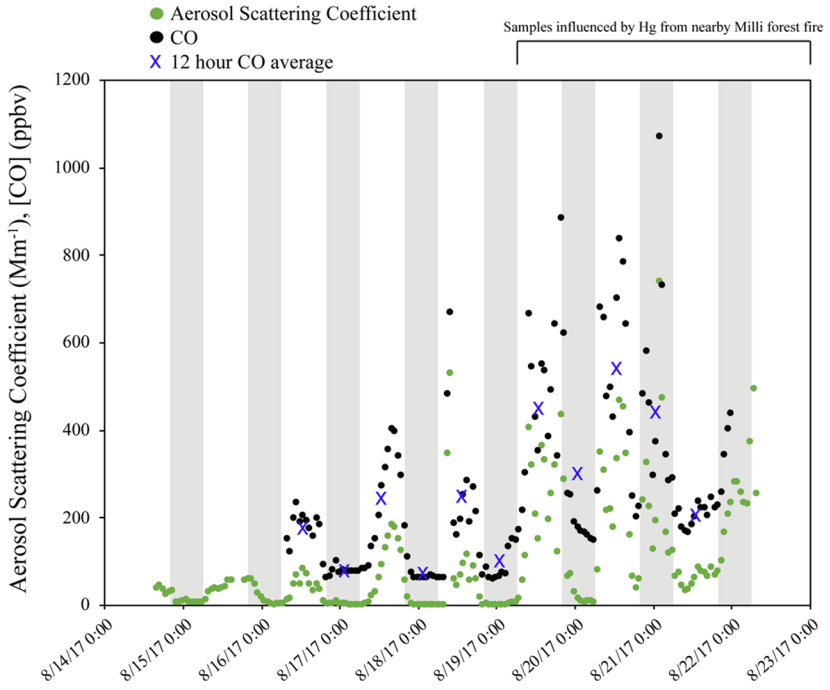

Figure 2. Aerosol scattering coefficient (Mm^{-1}) (green circles) and [CO] (ppbv) (black circles) as measured during the sampling campaign at MBO. Blue X represents 12 hour [CO] averages. Vertical gray shading represents nighttime periods and white represents daytime. The samples collected on Aug 19 through the end of the sampling period are dominated by Hg from the nearby Milli forest fire.

(A) and 1/THg vs Δ^{199}Hg on panel (B). We identify the three isotopic endmembers as follows:

Hg Re-emitted from Vegetation. The daytime samples fall along a mixing line between an endmember with high THg, low δ^{202}Hg, and intermediate Δ^{199}Hg and an endmember with intermediate THg, intermediate δ^{202}Hg, and low Δ^{199}Hg. We identify the high THg endmember as Hg^0 that has been re-emitted from vegetation through photoreduction of Hg^{II}. Yuan et al. demonstrated that the isotopic composition of Hg^0 re-emitted from vegetation is more negative in δ^{202}Hg and more positive in Δ^{199}Hg than ambient air with an offset of approximately −2.21 and +0.45‰ for δ^{202}Hg and Δ^{199}Hg, respectively.[47] This is consistent with photoreduction of Hg^{II} bound to reduced sulfur ligands.[57] Our samples do not display the same magnitude of difference between ambient air and re-emitted Hg^0, but this is expected because the experimental setup of Yuan et al. was designed to isolate the re-emitted Hg^0 from other processes.[47]

Unknown Low Δ^{199}Hg endmember. Previous studies have proposed that MIF occurring in the upper atmosphere (upper troposphere/lower stratosphere) can impart more negative MIF signatures on Hg^0 due to the increased exposure to UV radiation.[24] At sunrise as thermal convection begins in the valley at CD, there may be some downward mixing of overlying air into the valley with more negative Δ^{199}Hg values. However, mixing between the free troposphere and the planetary boundary layer would be expected to be minimal at CD. Additionally, the more negative Δ^{199}Hg values could be due to photoreduction of Hg bound to O/N functional groups, driving odd-MIF to more negative values compared with photoreduction from reduced sulfur ligands.[57] The relatively small number of samples collected makes it difficult to confidently identify this endmember.

Hg Modified by Uptake of Hg^0 by Vegetation. During the nighttime, the samples are influenced by an endmember with low THg, high δ^{202}Hg, and high Δ^{199}Hg. We identify this endmember as Hg^0 that has been modified by uptake into vegetation. As discussed earlier, uptake of Hg^0 by vegetation dominates during the nighttime hours in forested areas and preferentially takes up the light isotopes from the atmosphere. While the mechanism is unclear, Yuan et al. found that Hg^0 modified by the uptake of vegetation displays more positive δ^{202}Hg and more positive Δ^{199}Hg as compared to ambient air, which is consistent with the pattern we see for the nighttime samples. Additionally, Fu et al. attributed the shift in δ^{202}Hg and Δ^{199}Hg toward more positive values in Hg^0 collected during summer months to increased vegetation activity as compared to winter months. We propose that while the Hg^0 samples collected during the summer months are day and night integrations, they are somewhat analogous to our nighttime samples where increased uptake of Hg^0 by vegetation drives the isotopic composition toward more positive δ^{202}Hg and Δ^{199}Hg values.

While these three Hg endmembers can be generally identified by their distinct isotopic composition and THg, we highlight the need for additional sampling and experimental work to identify the fractionation mechanism that alters the isotopic composition of Hg^0 through the process of uptake by vegetation. Field measurements could consist of 12-h simultaneous Hg isotopic measurements at ground level, directly below the canopy and above the canopy. Additionally, simultaneous quantification and isotopic characterization of vegetation and soil fluxes could provide more insight into the relative contribution of each of the above processes.

3.3. Even-MIF at Camp Davis. Another useful tracer for identifying atmospheric Hg sources and/or transport distances is even-MIF. The fractionation process imparting even-MIF signatures on Hg is not well understood but it has been suggested to be related to photoinitiated oxidation occurring in the upper troposphere or lower stratosphere.[24] Multiple

https://dx.doi.org/10.1021/acs.est.0c01918
Environ. Sci. Technol. 2020, 54, 10502−10513

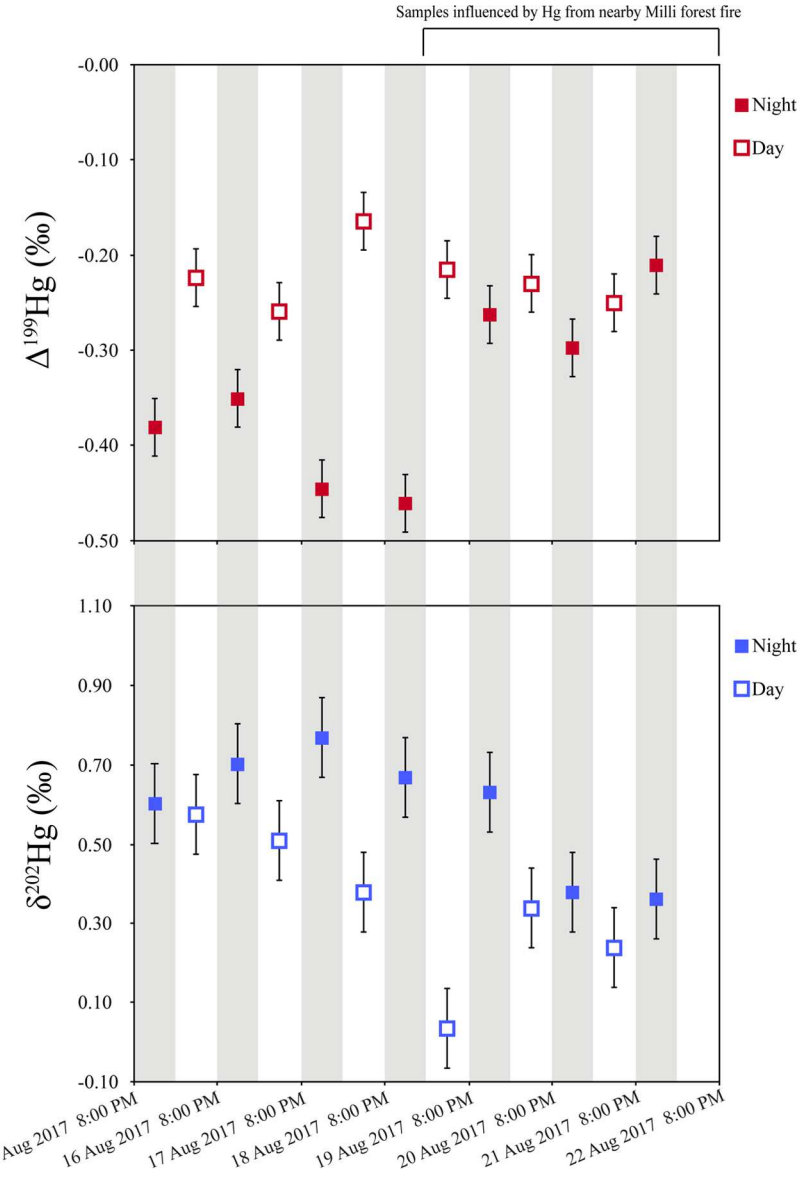

Figure 3. Mount Bachelor Hg isotope data plotted with δ^{202}Hg and Δ^{199}Hg on separate y-axes while sharing time on the *x*-axis. Vertical gray shading represents nighttime periods and white represents daytime. The black bars represent analytical error (2SD). The samples collected on Aug 19 through the end of the sampling period are dominated by Hg from the nearby Milli forest fire.

studies of atmospheric Hg samples reveal that samples with Hg dominantly in the oxidized form (Hg^{II}) display positive Δ^{200}Hg (average = 0.16 ± 0.13‰, 1 SD, n = 188)[19−21,24,58−63] while samples with Hg dominantly in the reduced form (Hg^0) display near zero or slightly negative Δ^{200}Hg (average = −0.06 ± 0.05‰, 1 SD, n = 154).[9,10,19,20,33,64−67] Hg^0 measured at CD reveals an average Δ^{200}Hg value of −0.09 ± 0.03‰ (1 SD, n = 6) for daytime samples and −0.07 ± 0.03‰ (1 SD, n = 7) for nighttime samples (Figure S7). CD samples reveal no statistical variation between day and night samples throughout the entire sampling period for Δ^{200}Hg (Table S2). Our measured Δ^{200}Hg values are consistent with all previously reported Hg^0 measurements (Table S2).[9,10,19,20,33,64−67]

3.4. Mount Bachelor THg Concentrations and Atmospheric Characterization. Hg^0 THg concentrations measured at MBO display slightly higher values (though not significantly different) during the day (average = 1.56 ± 0.19 ng/m^3, 1 SD, n = 6) than at night (average = 1.47 ± 0.27 ng/m^3, 1 SD, n = 7) (Figure S2B). Near the end of the sampling period during the night of Aug 20, the pattern reversed and THg concentrations were higher during the night than during the day. Starting on Aug 13, 2017, a forest fire, named the Milli Fire, ignited approximately 31 km NW of MBO and grew in size through the sampling period. The origin of air masses between day and night samples and throughout the entire sampling period suggests a dominant regional origin of air masses to the MBO sampling site (Figure S8). The back trajectories also indicate that the modeled air masses passed over the site of the Milli fire and, therefore, this added source of Hg may have become dominant near the end of the sampling period as discussed below. When we compare daytime THg concentrations, prior to the time when fire impacted the samples, to nighttime THg concentrations during the same time period, we find a statistically significant difference (Table S2).

https://dx.doi.org/10.1021/acs.est.0c01918
Environ. Sci. Technol. 2020, 54, 10502−10513

3.4.1. Identification of FT Air masses. Previous studies have used approaches of both direct measurements and modeling to understand the vertical profile of Hg species in the atmosphere. It has been proposed that while overall THg decreases with increasing altitude, there is also a decrease in Hg^0 THg concentrations with increasing altitude due to an increase in Hg oxidation and sorption of $Hg_{(g)}^{II}$ to atmospheric particles, which is known to increase with decreasing temperature.[68−70] Since MBO receives FT air masses at night, we hypothesize that the lower Hg^0 concentration measurements observed in the nighttime MBO samples are due to air masses from higher in the atmosphere exhibiting a shift in Hg speciation from Hg^0 to Hg^{II}.[28,71] This hypothesis is further supported by measurements of CO and aerosol scattering coefficient (Figure 2). Based on previous long-term measurements, it is well known that FT air masses at MBO are characterized by CO concentrations below 150 ppbv with concurrent aerosol scattering values <20 Mm^{-1} between 20:00 and 08:00 hours local time.[29,31,72,73] Using these thresholds to identify periods when FT air masses dominate, we identify the nights of Aug 15 through 18th as periods of influence from FT air masses. During each of these nights, there also appears to be some influence from the forest fires between 20:00 and 02:00−04:00 hours, keeping CO concentrations slightly elevated above 150 ppbv before decreasing below this threshold in the early morning hours. These nightly samples also display 4 of the 6 lowest Hg^0 THg concentrations measured during the sampling campaign (1.16−1.47 ng/m^3).

3.4.2. Identification of Forest Fire Influence at MBO. Beginning during the day on Aug 19, daytime CO concentrations consistently exceeded 400 ppbv with concurrent aerosol scattering values of >200 Mm^{-1}. Unlike earlier in the sampling period, CO concentrations and aerosol scattering values did not return to background values during the nighttime but rather stayed elevated above 140 ppbv and 50 Mm^{-1}, respectively. We suggest that these elevated values are consistent with a direct impact from the nearby forest fire. Due to the proximity of the Milli fire to MBO, it is likely that the smoke was transported to the sampling site within the PBL. From Aug 19 through the end of the sampling period, CO concentrations and aerosol scattering values did not reflect FT air masses during the nighttime but rather the transport of smoke plumes from the nearby forest fires, which came to dominate the Hg transported to MBO. Additionally, we use the relationship of THg concentration to CO concentration to characterize the change in Hg sources. As CO was measured continuously and Hg isotope samples are integrated over 12-h, we calculated 12-h average CO concentrations for comparison over the same time period as Hg samples were collected. We find that the [THg]/[CO] ratio significantly decreased from before the forest fire dominated the samples to when the samples were influenced by the fire (Table S2). This change in Hg source was more significant when comparing the nighttime samples prior to fire influence to the nighttime samples dominated by Hg from the forest fire (Table S2). Further discussion on this hypothesis that incorporates observed variations in the Hg isotopic composition of the samples is provided below.

3.5. Isotopic Characterization of Hg^0 at Mount Bachelor. We observed diel variation in the δ^{202}Hg values at MBO; however, the offset from each day to night throughout the sampling campaign was inconsistent and disappeared later in the sampling campaign due to the wildfire impact. Average δ^{202}Hg values throughout the entire sampling period during the day were 0.34 ± 0.19‰ (1 SD, n = 6), while nighttime average δ^{202}Hg values were 0.58 ± 0.16‰ (1 SD, n = 7) (Figure 3). When comparing the δ^{202}Hg values between the day and night samples, we find that they are statistically different (Table S2). Throughout the entire sampling period, the δ^{202}Hg values decrease from 0.60 ± 0.10‰ on the first night of sampling, Aug 15, to 0.36 ± 0.10‰ on the final night of sampling, Aug 21.

Similar to δ^{202}Hg, we observed diel variation in odd-MIF with more negative values at night (average Δ^{199}Hg = −0.35 ± 0.09‰, average Δ^{201}Hg = −0.30 ± 0.12‰, 1 SD, n = 7) than during the day (average Δ^{199}Hg = −0.22 ± 0.03‰, average Δ^{201}Hg = −0.17 ± 0.07‰, 1 SD, n = 6) (Figure 3). Daytime and nighttime samples are statistically different from each other for both Δ^{199}Hg and Δ^{201}Hg (Table S2). Similar to the variation in δ^{202}Hg observed at MBO, the variation in odd-MIF between the day and night samples at MBO disappeared starting on Aug 19 through the end of the sampling period.

3.5.1. Photochemical reduction of Hg^{II}. The ratios of Δ^{199}Hg to Δ^{201}Hg were determined for all MBO samples, only nighttime samples, and only daytime samples. A York regression was used with calculated slopes of 0.24 ± 0.12 (p < 0.01), 0.08 ± 0.21 (p < 0.01), and 0.03 ± 0.36 (p > 0.6), respectively. While the relationships between Δ^{199}Hg and Δ^{201}Hg are significant for all MBO samples and nighttime samples, the calculated slopes are much lower than those for any known reaction including photochemical reduction of Hg^{II}. The calculated slopes probably result from a mixture of different reactions and source mixing, though based on the calculated slopes, we can rule out in situ photochemical reduction of Hg^{II} as the dominant reaction driving the observed variation in odd-MIF at MBO.

3.5.2. Three-Endmember Mixing Model. At MBO, the full range in the isotopic composition of the Hg^0 samples collected can be accounted for through a three-endmember mixing model (Figure S9). Ancillary atmospheric measurements (CO and particle scattering) allowed us to identify the influence of distinct air masses and we now extrapolate that to the isotopic composition of Hg^0.

Free Tropospheric Endmember. On the nights of Aug 15−18, we identified influence from the free troposphere. The composition of Hg^0 in the free troposphere has intermediate THg (1.32 ± 0.13 ng/m^3, 1 SD, n = 3), high δ^{202}Hg (0.68 ± 0.07‰, 1 SD, n = 3), and low Δ^{199}Hg (−0.41 ± 0.05‰, 1 SD, n = 3). As previously discussed, Hg in the upper atmosphere may experience increased exposure to UV radiation, causing more MIF.[24] The direction of odd-MIF is determined by the binding ligands.[57] More negative Δ^{199}Hg values in Hg^0 as observed during FT influence at MBO are indicative of photoreduction of Hg^{II} from O/N functional groups. Additionally, we report what we believe to be most negative Δ^{199}Hg and Δ^{201}Hg values ever measured in Hg^0 (with values of −0.46 ± 0.05 and −0.50 ± 0.05‰, respectively) on the night of Aug 18 when MBO was receiving air masses from the FT.

Regional Background Endmember. Prior to influence from the nearby forest fire, the samples collected during the day have intermediate THg (1.15 ± 0.04 ng/m^3, 1 SD, n = 3), intermediate δ^{202}Hg (0.48 ± 0.10‰, 1 SD, n = 3), and high Δ^{199}Hg (−0.22 ± 0.05‰, 1 SD, n = 3). This endmember is most likely representative of regional Hg sources transported to MBO in the PBL that may be influenced by fractionation processes during transport, obscuring the initial isotopic

https://dx.doi.org/10.1021/acs.est.0c01918
Environ. Sci. Technol. 2020, 54, 10502−10513

composition of the source. Tang et al. demonstrated that the δ^{202}Hg of Hg^0 emitted from coal fired power plants can be enriched in δ^{202}Hg by up to ~2.5‰ as compared to the isotopic composition of feed coal with no associated MIF. While dependent on the initial isotopic composition, Hg^0 emissions from coal fired power plants were estimated to have a δ^{202}Hg value of 0.54 ± 0.25‰, (1 SD, n = 5), which is consistent with the δ^{202}Hg value of the identified regional background endmember.[74] Coal from the US has an average Δ^{199}Hg of −0.10 ± 0.13‰ (1 SD, n = 27),[75] which overlaps with the identified endmember. However, additional studies have identified smaller differences between δ^{202}Hg of feed coal and emitted Hg^0.[76] Additionally, atmospheric fractionation processes such as the uptake of Hg^0 by vegetation could fractionate the isotopes, obscuring the initial isotopic composition of released Hg^0 during transport to MBO.

Fire Endmember. As discussed above, from Aug 19 through the end of the sampling period, the isotopic composition of Hg^0 at MBO was influenced by the nearby Milli forest fire. We identify the forest fire endmember based on daytime measurements of Hg^0 impacted by the Milli fire as high THg (1.59 ± 0.21 ng/m^3, 1 SD, n = 3), low δ^{202}Hg (0.20 ± 0.16‰, 1 SD, n = 3), and high Δ^{199}Hg (−0.23 ± 0.02‰, 1 SD, n = 3). The isotopic composition of Hg in vegetation and litter has characteristically low δ^{202}Hg and negative Δ^{199}Hg (avg. δ^{202}Hg = −2.56 ± 0.64‰ and avg. Δ^{199}Hg −0.31 ± 0.13‰, 1 SD, n = 156)[20,25,66,77−80] and it is assumed that when vegetation is combusted, the light isotopes are preferentially released and MIF is conserved. The combustion of vegetation/litter does not have the associated MDF identified for coal combustion as the fractionation occurs due to the use of emissions control devices.[74] Ku et al. suggest that burning conditions, including O_2 availability, temperature, and burning duration, can affect Hg^0 volatilization in forest fires. This could account for some of the variability in δ^{202}Hg of Hg^0 observed at MBO in the samples impacted by the Milli fire as conditions changed through the sampling period. This variability could also be attributed to mixing with the other identified endmembers.

3.6. Even-MIF at Mount Bachelor. The samples collected at MBO during the daytime had an average Δ^{200}Hg value of −0.09 ± 0.02‰ (1 SD, n = 6) and those collected during the nighttime had an average Δ^{200}Hg value of −0.11 ± 0.05‰ (1 SD, n = 7) (Figure S10). There was no statistically significant variation in Δ^{200}Hg values between day and night samples (Table S2). To further assess the differences between Δ^{200}Hg values in the FT and the PBL, we compare the Δ^{200}Hg values in the nighttime samples prior to the forest fire's influence to the Δ^{200}Hg values in the daytime samples prior to the forest fire's influence (Table S2). Based on these relationships, we conclude that there is no statistical difference in even-MIF between FT air masses and PBL air masses measured at MBO. Furthermore, when we compare the average Δ^{200}Hg values from MBO to all published Hg^0/TGM data from other locations worldwide, we find a statistical difference (Table S2); however, none of our individual measured values are outside the range of previously measured values.[9,10,19,20,33,64−67] The difference between our measured Δ^{200}Hg values and those from previous studies may indicate that the high elevation of our study site captures lower Δ^{200}Hg values on average compared with samples collected at lower elevations.

Chen et al. documented extremely high positive Δ^{200}Hg values in precipitation (where Hg is expected to be dominated by Hg^{II}) reaching a maximum of 1.24‰. These authors attributed these high positive even-MIF values to photo-initiated oxidation in the tropopause. If high magnitude positive even-MIF is produced in Hg^{II} in the tropopause, we would expect there to be a residual pool of Hg^0 with more negative even-MIF. Since we found no statistical variation in the Δ^{200}Hg values in Hg^0 between FT and PBL air masses, we suggest that large-magnitude (negative Δ^{200}Hg for Hg^0 and positive Δ^{200}Hg for Hg^{II}) even-MIF may not be imparted on samples through reactions in the tropopause or it is also possible that events that mix Hg with large-magnitude even-MIF are stochastic and therefore these values are only rarely captured in measured samples.

■ ASSOCIATED CONTENT

Supporting Information

The Supporting Information is available free of charge at https://pubs.acs.org/doi/10.1021/acs.est.0c01918.

The supporting information contains a description of the mixing model used at Camp Davis, three data tables, a site map with sampling locations and regional point sources of mercury, and ten other supplemental figures (PDF)

■ AUTHOR INFORMATION

Corresponding Author

Aaron Y. Kurz − *Department of Earth and Environmental Sciences, University of Michigan, Ann Arbor, Michigan 48109, United States;* orcid.org/0000-0002-6729-1223; Email: kurz@umich.edu

Authors

Joel D. Blum − *Department of Earth and Environmental Sciences, University of Michigan, Ann Arbor, Michigan 48109, United States;* orcid.org/0000-0001-5389-8633

Lynne E. Gratz − *Environmental Studies Program, Colorado College, Colorado Springs, Colorado 80903, United States;* orcid.org/0000-0002-7904-991X

Daniel A. Jaffe − *School of Science, Technology, Engineering & Mathematics, University of Washington Bothell, Bothell, Washington 98011, United States;* orcid.org/0000-0003-1965-9051

Complete contact information is available at: https://pubs.acs.org/10.1021/acs.est.0c01918

Notes

The authors declare no competing financial interest.

■ ACKNOWLEDGMENTS

The authors thank Marcus Johnson for his guidance and help in operating the CV-MC-ICP-MS. The authors gratefully acknowledge the NOAA Air Resources Laboratory (ARL) for the provision of the HYSPLIT transport and dispersion model and READY website (https://www.ready.noaa.gov) used in this publication.

■ REFERENCES

(1) Mason, R.; Fitzgerald, W.; Morel, F. The Biogeochemical Cycling of Elemental Mercury: Anthropogenic Influences. *Geochim. Cosmochim. Acta* **1994**, *58*, 3191−3198.

(2) Obrist, D.; Kirk, J. L.; Zhang, L.; Sunderland, E. M.; Jiskra, M.; Selin, N. E. A Review of Global Environmental Mercury Processes in

Response to Human and Natural Perturbations: Changes of Emissions, Climate, and Land Use. *Ambio* **2018**, *47*, 116−140.
(3) Kurz, A. Y.; Blum, J. D.; Washburn, S. J.; Baskaran, M. Changes in the Mercury Isotopic Composition of Sediments from a Remote Alpine Lake in Wyoming, USA. *Sci. Total Environ.* **2019**, *669*, 973−982.
(4) Lindberg, S. E.; Stratton, W. J. Atmospheric Mercury Speciation: Concentrations and Behavior of Reactive Gaseous Mercury in Ambient Air. *Environ. Sci. Technol.* **1998**, *32*, 49−57.
(5) Schroeder, William H.; Munthe, J. Atmospheric Mercury - An Overview. *Atmos. Environ.* **1998**, *32*, 809−822.
(6) Slemr, F.; Angot, H.; Dommergue, A.; Magand, O.; Barret, M.; Weigelt, A.; Ebinghaus, R.; Brunke, E. G.; Pfaffhuber, K. A.; Edwards, G.; Howard, D.; Powell, J.; Keywood, M.; Wang, F. Comparison of Mercury Concentrations Measured at Several Sites in the Southern Hemisphere. *Atmos. Chem. Phys.* **2015**, *15*, 3125−3133.
(7) Ariya, P. A.; Skov, H.; Grage, M. M. L.; Goodsite, M. E. *Gaseous Elemental Mercury in the Ambient Atmosphere: Review of the Application of Theoretical Calculations and Experimental Studies for Determination of Reaction Coefficients and Mechanisms with Halogens and Other Reactants*; Elsevier Masson SAS: 2008; Vol. *55*.
(8) Subir, M.; Ariya, P. A.; Dastoor, A. P. A Review of the Sources of Uncertainties in Atmospheric Mercury Modeling II. Mercury Surface and Heterogeneous Chemistry - A Missing Link. *Atmos. Environ.* **2012**, *46*, 1−10.
(9) Demers, J. D.; Sherman, L. S.; Blum, J. D.; Marsik, F. J.; Dvonch, J. T. Coupling Atmospheric Mercury Isotope Ratios and Meteorology to Identify Sources of Mercury Impacting a Coastal Urban-Industrial Region near Pensacola, Florida, USA. *Global Biogeochem. Cycles* **2015**, *29*, 1689−1705.
(10) Fu, X.; Marusczak, N.; Wang, X.; Gheusi, F.; Sonke, J. E. Isotopic Composition of Gaseous Elemental Mercury in the Free Troposphere of the Pic Du Midi Observatory, France. *Environ. Sci. Technol.* **2016**, *50*, 5641−5650.
(11) Kwon, S. Y.; Selin, N. E. Uncertainties in Atmospheric Mercury Modeling for Policy Evaluation. *Curr. Pollut. Rep.* **2016**, *2*, 103−114.
(12) Blum, J. D.; Bergquist, B. A. Reporting of Variations in the Natural Isotopic Composition of Mercury. *Anal. Bioanal. Chem.* **2007**, *388*, 353−359.
(13) Yin, R.; Feng, X.; Shi, W. Application of the Stable-Isotope System to the Study of Sources and Fate of Hg in the Environment: A Review. *Appl. Geochem.* **2010**, *25*, 1467−1477.
(14) Kritee, K.; Blum, J. D.; Barkay, T. Mercury Stable Isotope Fractionation during Reduction of Hg (II) by Different Microbial Pathways Mercury Stable Isotope Fractionation during Reduction of Hg (II) by Different Microbial Pathways. *Environ. Sci. Technol.* **2008**, *42*, 9171−9177.
(15) Kritee, K.; Barkay, T.; Blum, J. D. Mass Dependent Stable Isotope Fractionation of Mercury during Mer Mediated Microbial Degradation of Monomethylmercury. *Geochim. Cosmochim. Acta* **2009**, *73*, 1285−1296.
(16) Wiederhold, J. G.; Cramer, C. J.; Daniel, K.; Infante, I.; Bourdon, B.; Kretzschmar, R. Equilibrium Mercury Isotope Fractionation between Dissolved Hg(II) Species and Thiol-Bound Hg. *Environ. Sci. Technol.* **2010**, *44*, 4191−4197.
(17) Chandan, P.; Ghosh, S.; Bergquist, B. A. Mercury Isotope Fractionation during Aqueous Photoreduction of Monomethylmercury in the Presence of Dissolved Organic Matter. *Environ. Sci. Technol.* **2015**, *49*, 259−267.
(18) Rose, C. H.; Ghosh, S.; Blum, J. D.; Bergquist, B. A. Effects of Ultraviolet Radiation on Mercury Isotope Fractionation during Photo-Reduction for Inorganic and Organic Mercury Species. *Chem. Geol.* **2015**, *405*, 102−111.
(19) Gratz, L. E.; Keeler, G. J.; Blum, J. D.; Sherman, L. S. Isotopic Composition and Fractionation of Mercury in Great Lakes Precipitation and Ambient Air. *Environ. Sci. Technol.* **2010**, *44*, 7764−7770.
(20) Demers, J. D.; Blum, J. D.; Zak, D. R. Mercury Isotopes in a Forested Ecosystem: Implications for Air-Surface Exchange Dynamics and the Global Mercury Cycle. *Global Biogeochem. Cycles* **2013**, *27*, 222−238.
(21) Yuan, S.; Chen, J.; Cai, H.; Yuan, W.; Wang, Z.; Huang, Q.; Liu, Y.; Wu, X. Sequential Samples Reveal Significant Variation of Mercury Isotope Ratios during Single Rainfall Events. *Sci. Total Environ.* **2018**, *624*, 133−144.
(22) Talbot, R.; Mao, H.; Scheuer, E.; Dibb, J.; Avery, M. Total Depletion of Hg ° in the Upper Troposphere − Lower Stratosphere. *Geophys. Res. Lett.* **2007**, *34*, 1−5.
(23) Slemr, F.; Weigelt, A.; Ebinghaus, R.; Kock, H. H.; Bödewadt, J.; Brenninkmeijer, C. A. M.; Rauthe-Schöch, A.; Weber, S.; Hermann, M.; Becker, J.; Zahn, A.; Martinsson, B. Atmospheric Mercury Measurements Onboard the CARIBIC Passenger Aircraft. *Atmos. Meas. Tech.* **2016**, *9*, 2291−2302.
(24) Chen, J.; Hintelmann, H.; Feng, X.; Dimock, B. Unusual Fractionation of Both Odd and Even Mercury Isotopes in Precipitation from Peterborough, ON, Canada. *Geochim. Cosmochim. Acta* **2012**, *90*, 33−46.
(25) Enrico, M.; Roux, G. Le.; Marusczak, N.; Heimbürger, L.-E.; Claustres, A.; Fu, X.; Sun, R.; Sonke, J. E. Atmospheric Mercury Transfer to Peat Bogs Dominated by Gaseous Elemental Mercury Dry Deposition. *Environ. Sci. Technol.* **2016**, *50*, 2405−2412.
(26) Huang, Q.; Chen, J.; Huang, W.; Reinfelder, J. R.; Fu, P.; Yuan, S.; et al. Diel Variation in Mercury Stable Isotope Ratios Records Photoreduction of PM2.5-Bound Mercury. *Atmos. Chem. Phys.* **2019**, *19*, 315−325.
(27) Jiskra, M.; E. Sonke, J.; Agnan, Y.; Helmig, D.; Obrist, D. Insights from Mercury Stable Isotopes on Terrestrial-Atmosphere Exchange of Hg(0) in the Arctic Tundra. *Biogeosciences* **2019**, *16*, 4051−4064.
(28) Swartzendruber, P. C.; Jaffe, D. A.; Prestbo, E. M.; Weiss-Penzias, P.; Selin, N. E.; Park, R.; Jacob, D. J.; Strode, S.; Jaeglé, L. Observations of Reactive Gaseous Mercury in the Free Troposphere at the Mount Bachelor Observatory *J. Geophys. Res. Atmos.* 2006, *11*124 DOI: 10.1029/2006JD007415.
(29) Weiss-Penzias, P.; Jaffe, D. A.; Swartzendruber, P.; Dennison, J. B.; Chand, D.; Hafner, W.; Prestbo, E. Observations of Asian Air Pollution in the Free Troposphere at Mount Bachelor Observatory during the Spring of 2004 *J. Geophys. Res.* 2006, *111*, DOI: 10.1029/2005JD006522.
(30) Jaffe, D.; Prestbo, E.; Swartzendruber, P.; Weiss-Penzias, P.; Kato, S.; Takami, A.; Hatakeyama, S.; Kajii, Y. Export of Atmospheric Mercury from Asia. *Atmos. Environ.* **2005**, *39*, 3029−3038.
(31) Ambrose, J. L.; Reidmiller, D. R.; Jaffe, D. A. Causes of High O3 in the Lower Free Troposphere over the Pacific Northwest as Observed at the Mt. Bachelor Observatory. *Atmos. Environ.* **2011**, *45*, 5302−5315.
(32) Finley, B. D.; Swartzendruber, P. C.; Jaffe, D. A. Particulate Mercury Emissions in Regional Wildfire Plumes Observed at the Mount Bachelor Observatory. *Atmos. Environ.* **2009**, *43*, 6074−6083.
(33) Fu, X.; Yang, X.; Tan, Q.; Ming, L.; Lin, T.; Lin, C.-J.; Li, X.; Feng, X. Isotopic Composition of Gaseous Elemental Mercury in the Marine Boundary Layer of East China Sea. *J. Geophys. Res. Atmos.* **2018**, *123*, 7656−7669.
(34) Blum, J. D.; Johnson, M. W. Recent Developments in Mercury Stable Isotope Analysis. *Rev. Mineral. Geochem.* **2017**, *82*, 733−757.
(35) Swartzendruber, P. C.; Chand, D.; Jaffe, D. A.; Smith, J.; Reidmiller, D.; Gratz, L.; Keeler, J.; Strode, S.; Jaeglé, L.; Talbot, R. Vertical Distribution of Mercury, CO, Ozone, and Aerosol Scattering Coefficient in the Pacific Northwest during the Spring 2006 INTEX-B Campaign. *J. Geophys. Res. Atmos* **2008**, *113*, 1−15.
(36) Fischer, E. V.; Perry, K. D.; Jaffe, D. A. Optical and Chemical Properties of Aerosols Transported to Mount Bachelor during Spring 2010. *J. Geophys. Res. Atmos.* **2011**, *116*, 1−13.
(37) Zhang, L.; Jaffe, D. A. Trends and Sources of Ozone and Sub-Micron Aerosols at the Mt. Bachelor Observatory (MBO) during 2004−2015. *Atmos. Environ.* **2017**, *165*, 143−154.
(38) Stein, A. F.; Draxler, R. R.; Rolph, G. D.; Stunder, B. J. B.; Cohen, M. D.; Ngan, F. Noaa's Hysplit Atmospheric Transport and

Dispersion Modeling System. *Bull. Am. Meteorol. Soc.* **2015**, *96*, 2059−2077.
(39) Rolph, G.; Stein, A.; Stunder, B. Real-Time Environmental Applications and Display SYstem: READY. *Environ. Model. Softw.* **2017**, *95*, 210−228.
(40) Temme, C.; Blanchard, P.; Steffen, A.; Banic, C.; Beauchamp, S.; Poissant, L.; Tordon, R.; Wiens, B. Trend, Seasonal and Multivariate Analysis Study of Total Gaseous Mercury Data from the Canadian Atmospheric Mercury Measurement Network (CAMNet). *Atmos. Environ.* **2007**, *41*, 5423−5441.
(41) Weigelt, A.; Ebinghaus, R.; Manning, A. J.; Derwent, R. G.; Simmonds, P. G.; Spain, T. G.; Jennings, S. G.; Slemr, F. Analysis and Interpretation of 18 Years of Mercury Observations since 1996 at Mace Head, Ireland. *Atmos. Environ.* **2015**, *100*, 85−93.
(42) Sprovieri, F.; Pirrone, N.; Bencardino, M.; Amore, F. D.; Carbone, F.; Cinnirella, S.; Mannarino, V.; Landis, M.; Weigelt, A.; Brunke, E.; Labuschagne, C.; Munthe, J.; Wängberg, I.; Artaxo, P.; Morais, F.; De, H.; et al. Atmospheric Mercury Concentrations Observed at Ground-Based Monitoring Sites Globally Distributed in the Framework of the GMOS Network. *Atmos. Chem. Phys.* **2016**, *16*, 11915−11935.
(43) Kellerhals, M.; Beauchamp, S.; Belzer, W.; Blanchard, P.; Froude, F.; Harvey, B.; McDonald, K.; Pilote, M.; Poissant, L.; Puckett, K.; Schroeder, B.; Steffen, A.; Tordon, R. Temporal and Spatial Variability of Total Gaseous Mercury in Canada: Results from the Canadian Atmospheric Mercury Measurement Network (CAMNet). *Atmos. Environ.* **2003**, *37*, 1003−1011.
(44) Poissant, L.; Pilote, M.; Yumvihoze, E.; Lean, D. Mercury Concentrations and Foliage/Atmosphere Fluxes in a Maple Forest Ecosystem in Québec, Canada. *J. Geophys. Res. Atmos.* **2008**, *113*, 1−12.
(45) Fu, X.; Zhu, W.; Zhang, H.; Sommar, J.; Yu, B.; Yang, X.; Wang, X.; Lin, C. J.; Feng, X. Depletion of Atmospheric Gaseous Elemental Mercury by Plant Uptake at Mt. Changbai, Northeast China. *Atmos. Chem. Phys.* **2016**, *16*, 12861−12873.
(46) Jiskra, M.; Sonke, J. E.; Obrist, D.; Bieser, J.; Ebinghaus, R.; Myhre, C. L.; Pfaffhuber, K. A.; Wängberg, I.; Kyllönen, K.; Worthy, D.; Martin, L. G.; Labuschagne, C.; Mkololo, T.; Ramonet, M.; Magand, O.; Dommergue, A. A Vegetation Control on Seasonal Variations in Global Atmospheric Mercury Concentrations. *Nat. Geosci.* **2018**, *11*, 244−251.
(47) Yuan, W.; Sommar, J.; Lin, C.; Wang, X.; Li, K.; Liu, Y.; Zhang, H.; Lu, Z.; Wu, C.; Feng, X. Stable Isotope Evidence Shows Re-Emission of Elemental Mercury Vapor Occurring after Reductive Loss from Foliage. *Environ. Sci. Technol.* **2019**, *53*, 651−660.
(48) Fu, X.; Zhang, H.; Liu, C.; Zhang, H.; Lin, C. J.; Feng, X. Significant Seasonal Variations in Isotopic Composition of Atmospheric Total Gaseous Mercury at Forest Sites in China Caused by Vegetation and Mercury Sources. *Environ. Sci. Technol.* **2019**, *53*, 13748−13756.
(49) Talbot, R.; Mao, H.; Sive, B. Diurnal Characteristics of Surface Level O3 and Other Important Trace Gases in New England. *J. Geophys. Res. Atmos.* **2005**, *110*, 1−16.
(50) Wehr, R.; Commane, R.; Munger, J. W.; Barry Mcmanus, J.; Nelson, D. D.; Zahniser, M. S.; Saleska, S. R.; Wofsy, S. C. Dynamics of Canopy Stomatal Conductance, Transpiration, and Evaporation in a Temperate Deciduous Forest, Validated by Carbonyl Sulfide Uptake. *Biogeosciences* **2017**, *14*, 389−401.
(51) Mao, H.; Talbot, R. W.; Sigler, J. M.; Sive, B. C.; Hegarty, J. D. Seasonal and Diurnal Variations of Hg ° over New England. *Atmos. Chem. Phys.* **2008**, *8*, 1403−1421.
(52) Bergquist, B. A.; Blum, J. D. Mass-Dependent and -Independent Fractionation of Hg Isotopes by Photoreduction in Aquatic Systems. *Science* **2007**, *318*, 417−420.
(53) Sun, G.; Sommar, J.; Feng, X.; Lin, C.-J.; Ge, M.; Wang, W.; Yin, R.; Fu, X.; Shang, L. Mass-Dependent and -Independent Fractionation of Mercury Isotope during Gas-Phase Oxidation of Elemental Mercury Vapor by Atomic Cl and Br. *Environ. Sci. Technol.* **2016**, *50*, 9232−9241.
(54) York, D. Least Squares Fitting of a Straight Line with Correlated Errors. *Earth Planet. Sci. Lett.* **1968**, *5*, 320−324.
(55) Donovan, P. M.; Blum, J. D.; Demers, J. D.; Gu, B.; Brooks, S. C.; Peryam, J. Identification of Multiple Mercury Sources to Stream Sediments near Oak Ridge, TN, USA. *Environ. Sci. Technol.* **2014**, *48*, 3666−3674.
(56) Washburn, S. J.; Blum, J. D.; Kurz, A. Y.; Pizzuto, J. E. Spatial and Temporal Variation in the Isotopic Composition of Mercury in the South River, VA. *Chem. Geol.* **2018**, *494*, 96−108.
(57) Zheng, W.; Hintelmann, H. Isotope Fractionation of Mercury during Its Photochemical Reduction by Low-Molecular-Weight Organic Compounds. *J. Phys. Chem. A* **2010**, *114*, 4246−4253.
(58) Sherman, L. S.; Blum, J. D.; Keeler, G. J.; Demers, J. D.; Dvonch, J. T. Investigation of Local Mercury Deposition from a Coal-Fired Power Plant Using Mercury Isotopes. *Environ. Sci. Technol.* **2012**, *46*, 382−390.
(59) Sherman, L. S.; Blum, J. D.; Dvonch, J. T.; Gratz, L. E.; Landis, M. S. The Use of Pb, Sr, and Hg Isotopes in Great Lakes Precipitation as a Tool for Pollution Source Attribution. *Sci. Total Environ.* **2015**, *502*, 362−374.
(60) Donovan, P. M.; Blum, J. D.; Yee, D.; Gehrke, G. E.; Singer, M. B. An Isotopic Record of Mercury in San Francisco Bay Sediment. *Chem. Geol.* **2013**, *349*−*350*, 87−98.
(61) Wang, Z.; Chen, J.; Feng, X.; Hintelmann, H.; Yuan, S.; Cai, H.; Huang, Q.; Wang, S.; Wang, F. Mass-Dependent and Mass-Independent Fractionation of Mercury Isotopes in Precipitation from Guiyang, SW China. *Comptes Rendus - Geosci.* **2015**, *347*, 358−367.
(62) Huang, S.; Sun, L.; Zhou, T.; Yuan, D.; Du, B.; Sun, X. Natural Stable Isotopic Compositions of Mercury in Aerosols and Wet Precipitations around a Coal-Fired Power Plant in Xiamen, Southeast China. *Atmos. Environ.* **2018**, *173*, 72−80.
(63) Kritee, K.; Motta, L. C.; Blum, J. D.; Tsui, M. T.-K.; Reinfelder, J. R. Photomicrobial Visible Light-Induced Magnetic Mass Independent Fractionation of Mercury in a Marine Microalga. *ACS Earth Space Chem.* **2017**, *2*, 432−440.
(64) Sherman, L. S.; Blum, J. D.; Johnson, K. P.; Keeler, G. J.; Barres, Ja.; Douglas, Ta. Mass-Independent Fractionation of Mercury Isotopes in Arctic Snow Driven by Sunlight. *Nat. Geosci.* **2010**, *3*, 173−177.
(65) Rolison, J. M.; Landing, W. M.; Luke, W.; Cohen, M.; Salters, V. J. M. Isotopic Composition of Species-Specific Atmospheric Hg in a Coastal Environment. *Chem. Geol.* **2013**, *336*, 37−49.
(66) Yu, B.; Fu, X.; Yin, R.; Zhang, H.; Wang, X.; Lin, C.-J.; Wu, C.; Zhang, Y.; He, N.; Fu, P.; Wang, Z.; Shang, L.; Sommar, J.; Sonke, J. E.; Maurice, L.; Guinot, B.; Feng, X. Isotopic Composition of Atmospheric Mercury in China: New Evidence for Source and Transformation Processes in Air and in Vegetation. *Environ. Sci. Technol.* **2016**, *50*, 9262−9269.
(67) Yamakawa, A.; Moriya, K.; Yoshinaga, J. Determination of Isotopic Composition of Atmospheric Mercury in Urban-Industrial and Coastal Regions of Chiba, Japan, Using Cold Vapor Multi-collector Inductively Coupled Plasma Mass Spectrometry. *Chem. Geol.* **2017**, *448*, 84−92.
(68) Murphy, D. M.; Hudson, P. K.; Thomson, D. S.; Sheridan, P. J.; Wilson, J. C. Observations of Mercury-Containing Aerosols. *Environ. Sci. Technol.* **2006**, *40*, 3163−3167.
(69) Rutter, A. P.; Schauer, J. J. The Effect of Temperature on the Gas-Particle Partitioning of Reactive Mercury in Atmospheric Aerosols. *Atmos. Environ.* **2007**, *41*, 8647−8657.
(70) Lyman, S. N.; Jaffe, D. A. Formation and Fate of Oxidized Mercury in the Upper Troposphere and Lower Stratosphere. *Nat. Geosci.* **2012**, *5*, 114−117.
(71) Gratz, L. E.; Ambrose, J. L.; Jaffe, D. A.; Shah, V.; Jaeglé, L.; Stutz, J.; Festa, J.; Spolaor, M.; Tsai, C.; Selin, N. E.; Song, S.; Zhou, X.; Weinheimer, A. J.; Knapp, D. J.; Montzka, D. D.; Flocke, F. M.; Campos, T. L.; Apel, E.; Hornbrook, R.; Blake, N. J.; Hall, S.; Tyndall, G. S.; Reeves, M.; Stechman, D.; Stell, M. Oxidation of Mercury by

https://dx.doi.org/10.1021/acs.est.0c01918
Environ. Sci. Technol. 2020, 54, 10502−10513

Bromine in the Subtropical Pacific Free Troposphere. *Geophys. Res. Lett.* **2015**, *42*, 494−502.
(72) Weiss-Penzias, P.; Jaffe, D.; Swartzendruber, P.; Hafner, W.; Chand, D.; Prestbo, E. Quantifying Asian and Biomass Burning Sources of Mercury Using the Hg/CO Ratio in Pollution Plumes Observed at the Mount Bachelor Observatory. *Atmos. Environ.* **2007**, *41*, 4366−4379.
(73) Reidmiller, D. R.; Jaffe, D. A.; Fischer, E. V.; Finley, B. Nitrogen Oxides in the Boundary Layer and Free Troposphere at the Mt. Bachelor Observatory. *Atmos. Chem. Phys.* **2010**, *10*, 6043−6062.
(74) Tang, S.; Feng, C.; Feng, X.; Zhu, J.; Sun, R.; Fan, H.; Wang, L.; Li, R.; Mao, T.; Zhou, T. Stable Isotope Composition of Mercury Forms in Flue Gases from a Typical Coal-Fired Power Plant, Inner Mongolia, Northern China. *J. Hazard. Mater.* **2017**, *328*, 90−97.
(75) Sun, R.; Sonke, J. E.; Liu, G. Biogeochemical Controls on Mercury Stable Isotope Compositions of World Coal Deposits: A Review. *Earth-Sci. Rev.* **2016**, *152*, 1−13.
(76) Sun, R.; Sonke, J. E.; Heimbu, L.; Belkin, H. E.; Liu, G.; Shome, D.; Cukrowska, E.; Liousse, C.; Pokrovsky, O. S.; Streets, D. G. Mercury Stable Isotope Signatures of World Coal Deposits and Historical Coal Combustion Emissions. *Environ. Sci. Technol.* **2014**, *48*, 7660−7668.
(77) Zhang, H.; Yin, R.; Feng, X.; Sommar, J.; Anderson, C. W. N.; Sapkota, A.; Fu, X.; Larssen, T. Atmospheric Mercury Inputs in Montane Soils Increase with Elevation: Evidence from Mercury Isotope Signatures. *Sci. Rep.* **2013**, *3*, No. 3322.
(78) Jiskra, M.; Wiederhold, J. G.; Skyllberg, U.; Kronberg, R.-M.; Hajdas, I.; Kretzschmar, R. Mercury Deposition and Re-Emission Pathways in Boreal Forest Soils Investigated with Hg Isotope Signatures. *Environ. Sci. Technol.* **2015**, *49*, 7188−7196.
(79) Zheng, W.; Obrist, D.; Weis, D.; Bergquist, B. A. Mercury Isotope Compositions across North American Forests. *Biogeochem. Cycles* **2016**, *30*, 1475−1492.
(80) Wang, X.; Luo, J.; Yin, R.; Yuan, W.; Lin, C.; Sommar, J.; Feng, X.; Wang, H.; Lin, C. Using Mercury Isotopes To Understand Mercury Accumulation in the Montane Forest Floor of the Eastern Tibetan Plateau. *Environ. Sci. Technol.* **2017**, *51*, 801−809.

https://dx.doi.org/10.1021/acs.est.0c01918
Environ. Sci. Technol. 2020, 54, 10502−10513